Fifth International Conference on Advanced COmputational Methods in ENgineering (ACOMEN 2011)
Liège, Belgium, 14-17 November 2011

A two-scale model predicting the mechanical sliding and opening behavior of grain boundaries in nanocrystalline solids

V. Péron-Lührs[1], A. Jérusalem[2], F. Sansoz [3], L. Stainier[4], L. Noels [1]

[1] ULg-Computational & Multiscale Mechanics of Materials, The University of Liège
Chemin des Chevreuils 1, B-4000 Liège, Belgium

[2] IMDEA Materials Institute
Calle Profesor Aranguren, s/n, Madrid 28040, Spain

[3] School of Engineering and Materials Science Program, The University of Vermont
Burlington, VT 05405 USA

[4] Institut de Recherche en Génie Civil et Mécanique (GeM, UMR 6183 CNRS), Ecole Centrale de Nantes
1 rue de la Noë, F-44321 Nantes cedex 3, France

e-mails: *{Vincent.Peron-Luhrs, L.Noels}@ulg.ac.be*

Résumé

In polycrystalline materials with nanosized grains smaller than 100 nm, the deformation mechanisms taking place at grain boundaries (GBs) become dominant compared to intragranular crystal plasticity. Recent studies have revealed that more accurate mechanical properties can be obtained by choosing the relevant GB character distribution (GBCD). We use here a numerical multiscale approach (an extension of a previous work [1]) to predict the mechanical behavior of nanostructured metals according to their GBCD composed of either high angle GBs (HAB) or low angle GBs (LAB). The quasicontinuum method (QC) is used to obtain the GB mechanical response at the nanoscale under simple shear (sliding part) and tensile load (opening part). These QC results are then used in a finite element code (direct numerical simulation-DNS) as GB constitutive models. This two-scale framework does not suffer from length scales limitations conventionally encountered when considering the two scales separately.

1 Introduction

Nanocrystalline (nc) materials, i.e. with grain sizes smaller than 100 nm, behave quite differently from their coarse-grained counterparts [3]. Their advantageous mechanical properties seems to be highly influenced by their grain boundary (GB) character distribution (GBCD) [4] and a predictive understanding of these properties remains elusive.

The present study aims at predicting the mechanical behavior of two specific GBCDs by using a 2-scale framework. The GBCD's specificities result in the appropriate integration of two types of GBs, low-angle grain boundaries (LAB) and high-angle grain boundaries (HAB). The 2-scale framework is as follows. We use the quasicontinuum method developed by Tadmor and co-workers [5] to perform QC simulations of GBs undergoing simple shear loads (sliding part) and tensile load (opening part). This first step allows to characterize the GB atomistic mechanical behavior according to their misorientations. The GB opening behavior is the same for all GBs and is taken from the QC tensile test of the GB $\Sigma 3(111)$. That is to say that the specific misorientations of each GB is not taken into account for the time being as in the sliding case. As a second step, we introduce these atomistic laws in a finite element code [6].

In a previous work [1], it was found that yield stresses were overvalued compared to experimental results when cleavage was omitted. We propose here to include a GB-cleavage law to

partially correct this problem. To illustrate the ability of the method to capture the influence of the GB deformation mechanisms on nc metals responses, quasi-static tensile tests are performed for three cases : nc copper with a 94% HAB texture, nc copper with a full LAB texture and nc copper with a 94% HAB texture including the GB-cleavage law.

2 Computational method

2.1 Continuum formulation

In this section we expose the constitutive model. The governing equations and kinematic assumptions of the direct numerical simulation (DNS) can be found elsewhere [1]. In particular the presence of embedded GBs is accounted for by an adequate discretization (see Figures 1c and 1d).

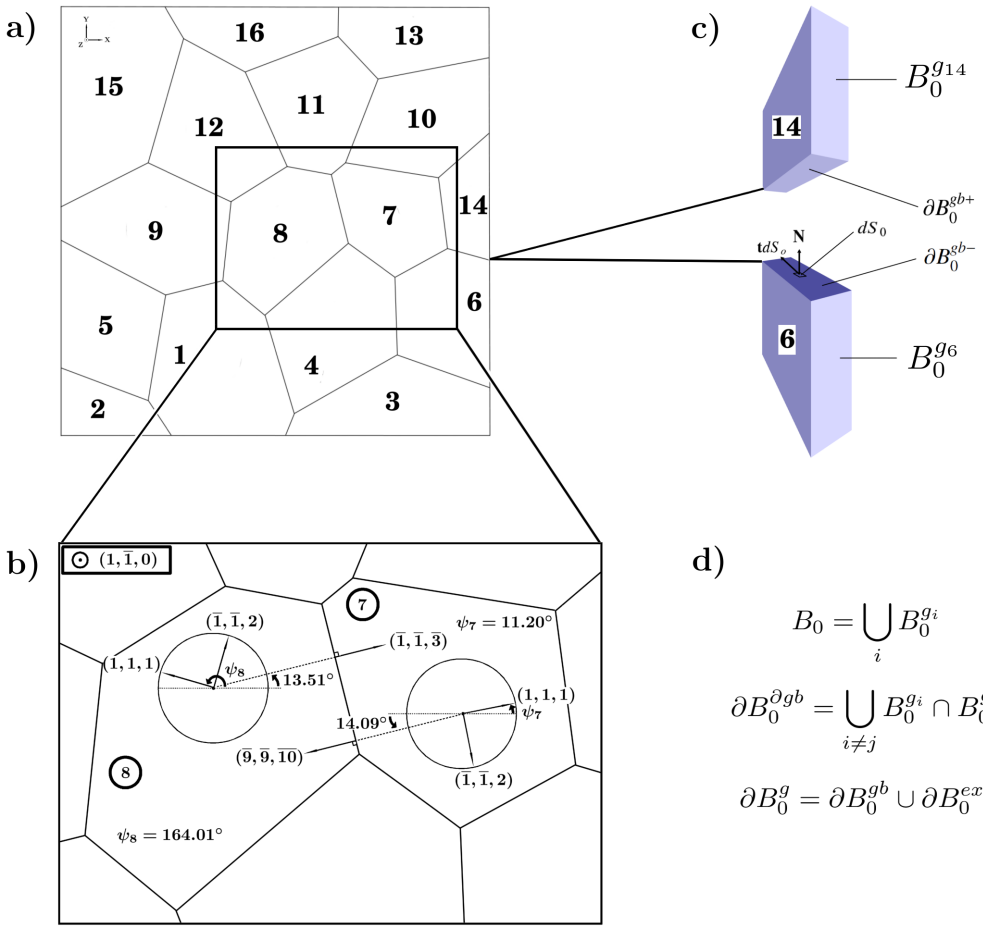

FIG. 1: a) Numbering of the nc grains. b) Illustration of orientation approach to reconstruct nc GBCD. c) and d) Schematics of geometric model of nc as a continuum with surfaces of discontinuity at GBs and related equations respectively.

2.1.1 Bulk constitutive model

In order to reveal the independent role played by GB deformation mechanisms, we will assume that the grain interiors can only undergo reversible elastic deformations [1]. The stress tensor can be decomposed into its a deviatoric and volumetric parts

$$\underline{\underline{\boldsymbol{\sigma}}} = \underline{\underline{\boldsymbol{s}}} + p\underline{\underline{\boldsymbol{I}}} \tag{1}$$

with

$$p = \frac{\sigma_{ii}}{3} = (\lambda + \frac{2G}{3})(\epsilon_{11} + \epsilon_{22} + \epsilon_{33}) = Ktr(\underline{\underline{\boldsymbol{\epsilon}}}) \tag{2}$$

and

$$\underline{\underline{\boldsymbol{s}}} = 2G\underline{\underline{\boldsymbol{\epsilon}}}^{dev} \tag{3}$$

where λ and G are the Lamé coefficients and K is the compression modulus.

2.1.2 Grain boundary constitutive model

We define the mean deformation mapping [7]

$$\underline{\tilde{\boldsymbol{\varphi}}} = \frac{1}{2}(\underline{\boldsymbol{\varphi}}^{+} + \underline{\boldsymbol{\varphi}}^{-}) \tag{4}$$

from which the original deformation mapping on both sides of the GB can be recovered as

$$\underline{\boldsymbol{\varphi}}^{\pm} = \underline{\tilde{\boldsymbol{\varphi}}} \pm \frac{1}{2}(\underline{\boldsymbol{\varphi}}^{+} - \underline{\boldsymbol{\varphi}}^{-}) = \underline{\tilde{\boldsymbol{\varphi}}} \pm \frac{1}{2}\underline{\boldsymbol{\delta}} \tag{5}$$

Where the displacement jump $\underline{\delta}$ is

$$\underline{\boldsymbol{\delta}} = [\![\underline{\boldsymbol{\varphi}}]\!] = \underline{\boldsymbol{\varphi}}^{+} - \underline{\boldsymbol{\varphi}}^{-} \tag{6}$$

Consequently, the deformed GB is defined as $S \equiv \tilde{\underline{\boldsymbol{\varphi}}}(S_0)$. Starting from a parametrization $\tilde{\underline{\boldsymbol{\varphi}}} = \tilde{\underline{\boldsymbol{\varphi}}}(s_\alpha), \alpha = 1, 2$ of S, it follows that the initial surface normal $\underline{\boldsymbol{N}}$ can be obtained directly from the covariant basis vectors $\underline{\boldsymbol{a}}_\alpha = \tilde{\underline{\boldsymbol{\varphi}}}_{0,\alpha}$ as

$$\underline{\boldsymbol{N}} = \frac{\underline{\boldsymbol{a}}_1 \times \underline{\boldsymbol{a}}_2}{\|\underline{\boldsymbol{a}}_1 \times \underline{\boldsymbol{a}}_2\|} \tag{7}$$

The displacement jumps may then be decomposed into an opening separation vector and a GB sliding vector, respectively as follows

$$\underline{\boldsymbol{\delta}}_n = (\underline{\boldsymbol{\delta}} \cdot \underline{\boldsymbol{N}})\underline{\boldsymbol{N}} = (\underline{\boldsymbol{N}} \otimes \underline{\boldsymbol{N}}) \cdot \underline{\boldsymbol{\delta}} \tag{8}$$

$$\underline{\boldsymbol{\delta}}_s = \underline{\boldsymbol{\delta}} - \underline{\boldsymbol{\delta}}_n = (\underline{\boldsymbol{I}} - \underline{\boldsymbol{N}} \otimes \underline{\boldsymbol{N}}) \cdot \underline{\boldsymbol{\delta}} \tag{9}$$

These kinematic assumptions lead to a constant state of deformation across the thickness h of the GB which can be expressed in the local orthonormal reference frame $(\underline{\boldsymbol{N}}_1, \underline{\boldsymbol{N}}_2, \underline{\boldsymbol{N}}_3) = ((\underline{\boldsymbol{a}}_1/|\underline{\boldsymbol{a}}_1|), (\underline{\boldsymbol{N}} \times \underline{\boldsymbol{a}}_1/|\underline{\boldsymbol{N}} \times \underline{\boldsymbol{a}}_1|), \underline{\boldsymbol{N}})$ as

$$\underline{\underline{\epsilon}} = \underbrace{\frac{\underline{\boldsymbol{\delta}}_n \cdot \underline{\boldsymbol{N}}_3}{h} \underline{\boldsymbol{N}}_3 \otimes \underline{\boldsymbol{N}}_3}_{\underline{\underline{\epsilon}}_n} + \underbrace{\frac{\underline{\boldsymbol{\delta}}_s \cdot \underline{\boldsymbol{N}}_1}{h} \frac{1}{2}(\underline{\boldsymbol{N}}_1 \otimes \underline{\boldsymbol{N}}_3 + \underline{\boldsymbol{N}}_3 \otimes \underline{\boldsymbol{N}}_1) + \frac{\underline{\boldsymbol{\delta}}_s \cdot \underline{\boldsymbol{N}}_2}{h} \frac{1}{2}(\underline{\boldsymbol{N}}_2 \otimes \underline{\boldsymbol{N}}_3 + \underline{\boldsymbol{N}}_3 \otimes \underline{\boldsymbol{N}}_2)}_{\underline{\underline{\epsilon}}_s} \tag{10}$$

It should be noted that h introduces a characteristic length scale in the model. The above expression also shows that the strain tensor additively decomposes in a sliding part $\underline{\underline{\epsilon_s}}$ and a normal opening part $\underline{\underline{\epsilon_n}}$.
Finally the traction is expressed as follows

$$\underline{\bar{t}} = h\underline{\underline{\boldsymbol{\sigma}}} \cdot \frac{\partial \underline{\underline{\epsilon}}}{\partial \underline{\delta}} \tag{11}$$

that can be simplified by using Equation (10) [6]

$$\underline{\bar{t}} = \underline{\underline{\boldsymbol{\sigma}}} \cdot \underline{\boldsymbol{N_3}} \tag{12}$$

As opposed to Jérusalem et al. [6], we assumed here that only the sliding component undergoes plastic deformation. Furthermore, in order to evaluate $\underline{\underline{\boldsymbol{\sigma}}}$ in Equation (11), we adopt the following model to describe GB plasticity

$$\sigma_p = \sigma_0(1 + \frac{\bar{\epsilon_p}}{\epsilon_0})^{\frac{1}{m}} \tag{13}$$

where σ_p is the yield stress corresponding to the equivalent plastic strain $\bar{\epsilon}_p$, σ_0 is the initial yield stress, m and ϵ_0 are parameters of the model.

In a recent work [1], GB opening deformation was considered to be elastic. We will reproduce in this paper the results obtained in this last study to assess the discrepancies when the GB-cleavage stress is integrated in the framework. The opening mechanical behavior takes into account a damage parameter D which is equal to 0 until the GB reaches a critical stress σ_c and is equal to 1 when the strain to failure δ_c is reached.

2.2 Quasicontinuum simulations

Instead of assigning a unique arbitrary constitutive GB law that is independent of the crystal misorientation, as in Ref. [6, 8], the shearing behavior of each GB is characterized here according to its structure using quasicontinuum (QC) simulations of tilt bicrystals undergoing simple shear loads. The QC method software used in the present study (available on www.qcmethod.com) was limited to two dimensions (2D) problems at 0 K. Every calculation was performed by projection of the 3D crystallography orientations along the GB tilt axis. The computational method used here to simulate the GB shearing can be found elsewhere [9, 1], see Figure 2.

The QC atomistic results (shear stress vs shear strain γ) were fitted to determine the finite element elasto-plastic parameters which are then used in the GBs constitutive laws of the direct numerical simulations. These parameters are the shear modulus G and the yield stress σ_0. The coefficients ϵ_0 and m are also parameters but remain constant for all GBs (1 and 1000 respectively). We assume here that the GB mechanical behavior is perfectly plastic. This procedure allows us to characterize the mechanical behaviors of all GBs. The corresponding results for GB_{12-9} (LAB texture) is given in Figure 3a. In that case, shear modulus is $G = 53$ GPa and maximum stress is $\sigma_0 = 4.18$ GPa. This fitting procedure was employed for each GB of the two textures studied.

The decohesion constitutive mechanical behavior is supposed to follow the $\Sigma3(111)$ behavior under tension. This last GB corresponds to a twin GB with a very low energy ($9mJ/m^2$). The $\Sigma3(111)$ parameters are found to be $\sigma_c = 10$ GPa and $\delta_c = 0.93$ nm. Figure 3b represents the normal displacement vs tensile stress for this GB under tensile loading. The QC computational method as regards to tensile loads can be found elsewhere [10].

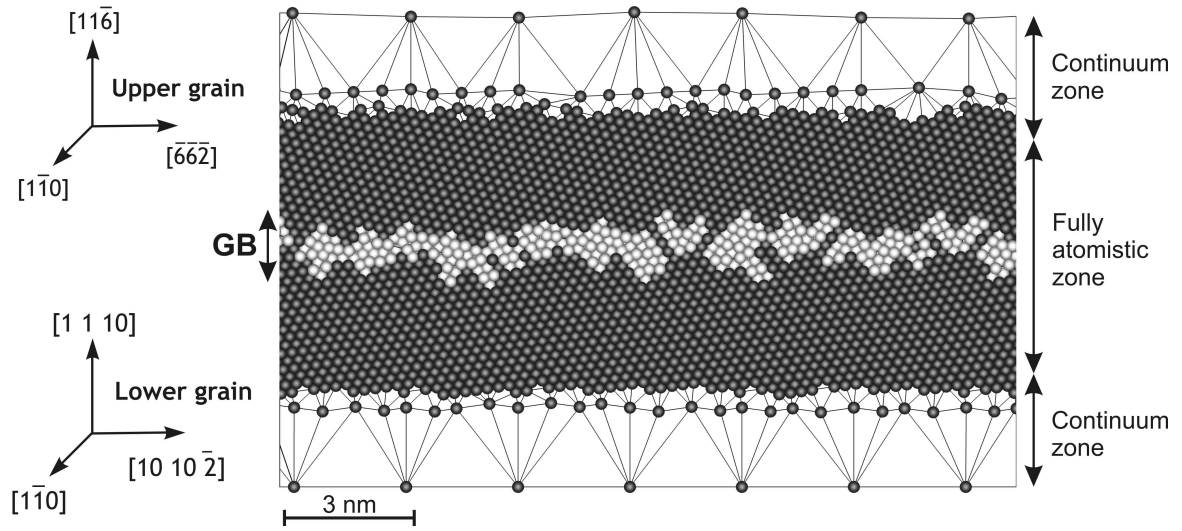

FIG. 2: Quasicontinuum model of GB_{10-7} in the high-angle texture. The continuum and the atomistic regions are indicated. The crystals orientation and GB position after relaxation are also shown. Atoms appearing in dark color present a perfect fcc stacking. Bright-colored atoms correspond to crystal defects.

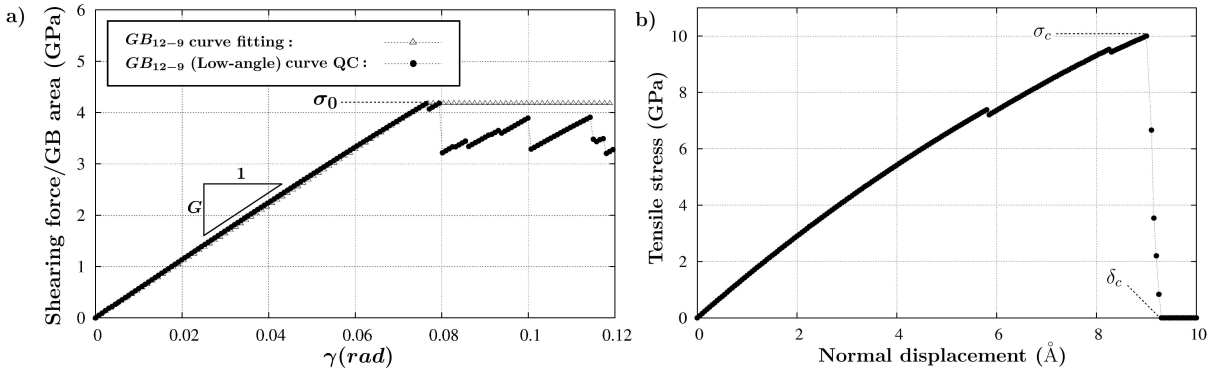

FIG. 3: a) Evolution of the shear stress as a function of applied shear strain for GB_{12-9}(LAB) fitted from QC simulation, b) Normal displacement vs tensile stress for a QC simulation of the strong GB Σ3(111). This opening behavior is adopted for all GBs.

2.3 Two-scale numerical simulations

In this framework, the two scales considered are the atomistic ($\approx$Å $\rightarrow$ QC) and the mesoscopic or upper scales (continuum). The calibration of the mechanical behavior at GBs in a nc solid (mesoscopic scale) is reached through QC simulations (atomistic scale). As seen before, the GB strain can be decomposed into two components : a sliding part and an opening part. In order to determine the sliding part, we perform QC simulations of GBs undergoing simple shear loads. On the other hand, the opening part, is considered to follow the very strong GB Σ3(111) mechanical behavior. Nevertheless, in the case of the comparison of the HA and LA textures, the GB-cleavage stress is not taken into account and the opening part is considered to follow an elastic behavior.

The nc solid studied here and illustrated on Figure 4a is composed of 16 grains and 34 GBs. Because this nc is composed of 34 GBs, 34 QC simulations are performed to obtain all the GBs mechanical behaviors. Two different textures, LAB en HAB, are studied here as described below.

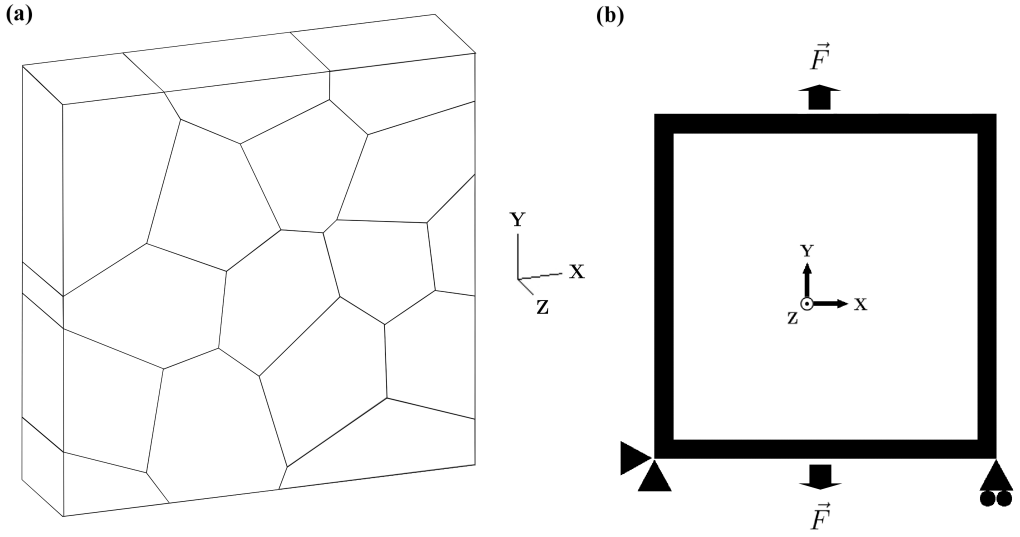

FIG. 4: Mesh and boundary conditions of tensile tests used for simulations. a) mesh with 16 grains. b) Boundary conditions for tensile tests.

2.4 Presentation of high-angle and low-angle textures

In order to reconstruct nc textures we use one representative volume element (RVE) finite element mesh (see Figure 4a). This RVE is 100 nm long along the X and Y axes and 25 nm long along the Z axis. This RVE (Figure 4a) consists of 16 grains, discretized in 7,451 tetrahedral elements and follows a Voronoï construction generated by an algorithm that checks if the grains sizes are homogeneous. All RVE grains are numbered as shown on Figure 1a so that each GB is determined by two numbers. For example, in Figure 1b, the interface between grains is defined as GB_{7-8}.

The aim of this part of the study is to illustrate the ability of this 2-scale method to model complex material behavior. We illustrate this ability through the study of two GBCDs. One contains only LABs and the other one 94% of HABs, the aim being to capture the mechanical behavior of nc metals according to their GBCD. Towards this end, we assign a grain orientation to each grain and plot misorientations distributions to determine LAB and HAB proportions.

Figure 1b illustrates the orientation approach used to reconstruct the nc HAB texture of the GB common to grains 7 and 8. The misorientation between both grains 7 and 8 is $\Delta\psi_{7-8} = |\psi_7 - \psi_8|$ with $\psi_7 = 11.20°$ and $\psi_8 = 164.01°$. ψ represents the misorientation of the basis vectors [1,1,1][$\overline{1}$,$\overline{1}$,2] around the out-of-plane axis [1,$\overline{1}$,0]. Rotation is positive counterclockwise and ranges from 0° to 360°. On the other hand, the difference $\Delta\psi$ represents the GB misorientation which is here the criterion determining if the GB considered belongs to HA or LA type. Each grain orientation allows us to characterize its GB normals. For instance, in the case of the GB_{7-8}, the normals at the interface from each 7th and 8th grain point of views are represented by the Miller indexes ($\overline{9}$,$\overline{9}$,$\overline{10}$) and ($\overline{1}$,$\overline{1}$,$\overline{3}$) respectively.

The misorientations belonging to the four intervals : 9°→81°, 99°→171°, 189°→261°, 279°→351° are considered HAB, the other ones belong to the LAB class, because of symmetry around the tilt axis. This symmetry allows us to present the misorientations distribution only from 0° to 90°. Figure 5 shows the misorientation distributions for both textures. For LA case, all misorientations belong to the interval from 0° to 9°, so that we can consider a 100% LAB GBCD. In the HAB case, only two GBs are low angles.

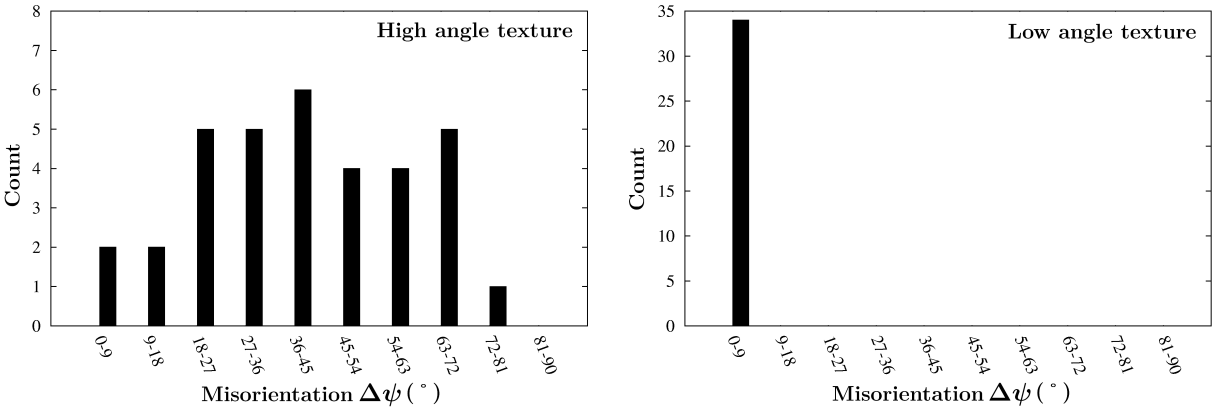

FIG. 5: Misorientations distributions for both textures HA and LA.

3 Results and discussion

3.1 Mechanical responses of HA and LA textures

The microstructure in Figure 1a is subjected to tensile tests. The boundary conditions are those applied in Figure 4b. During the tensile test, we calculate the average stress in the system as a function of the strain. Figure 6a shows the stress-strain curves of high angle and low angle textures under tension. A different mechanical behavior between HAB texture and LAB texture is observed. The yield stress of the HAB texture is smaller in the HAB case. 0.2% offset yield stresses of the HAB and the LAB texture are ≈ 4 GPa and ≈ 18 GPa respectively and the elastic deformation reached for these stresses are $\approx 3\%$ and $\approx 14\%$ respectively. These results are in relatively good agreement with dynamic molecular results [11] where a texture equivalent to a twin texture, i.e. with a similar mechanical behavior compared to LAB texture, reaches more than 12 GPa before entering in the plastic region appearing for a 7% strain. Also, in Ref. [12], nc composed of HAB are found to exhibit a yield stress of $\approx 2.7 - 3$ GPa for a 3% strain. Despite the fact that the yield stresses and their associated strains seem to be overvalued for the LAB texture, we observe nevertheless a definite trend in their mechanical behaviors. In the case of the LAB, the discrepancies are more pronounced than in the HAB case. Indeed, the LAB contribution to permanent deformation occurs later for LAB and should be accompanied by bulk plasticity, which would contribute to decrease the LAB texture yield stress obtained here.

Figure 6b shows the stress-strain curves of HA texture with and without decohesion law for GBs. This decohesion law ($\sigma_c = 10$ GPa, $\delta_c = 0.93$ nm) is computed atomistically with one QC simulation with a strong GB $\Sigma 3(111)$ and consequently with a low energy ($9J/m^2$). We note firstly a loss of strain energy in the case where GB-cleavage is incorporated into the microstructure. Then, the overall structure yield stress is found to be lower in this latter case due to the rapid activation of GB opening.

Figure 7 shows the plastic part of sliding vs total structure strain for the tensile test at four GB nodes in both cases (HA texture with and without cleavage law). For each node numbered from 1 to 4 and reported on Figure 7, we find that plasticity appears faster when the cleavage law is implemented. It is clear from Figure 7 that for each node the yield stresses have decreased substantially when the GB opening is not considered as being fully elastic. This results highlight the coupling between opening and sliding responses at GBs.

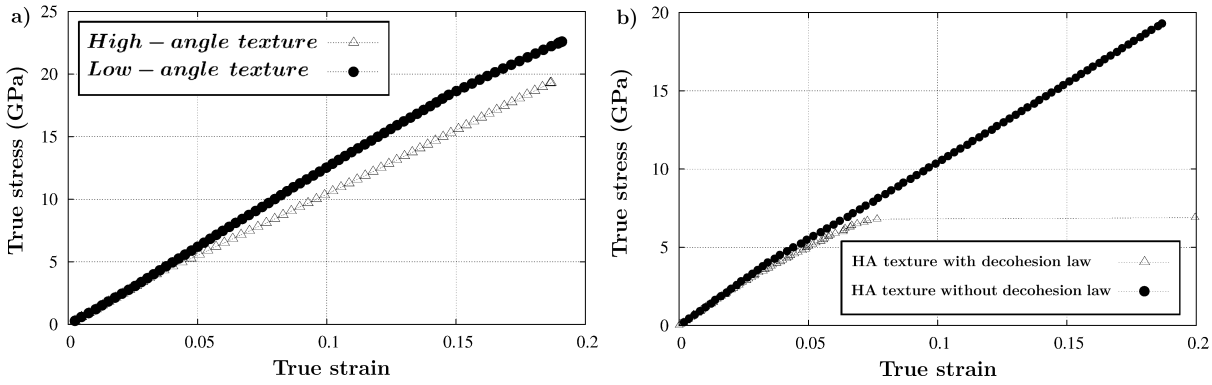

FIG. 6: a) Stress-strain curves of HAB and LAB textures nanostructures under tension. b) Stress-strain curves of HA texture nanostructure under tension with and without considering the GB decohesion behavior.

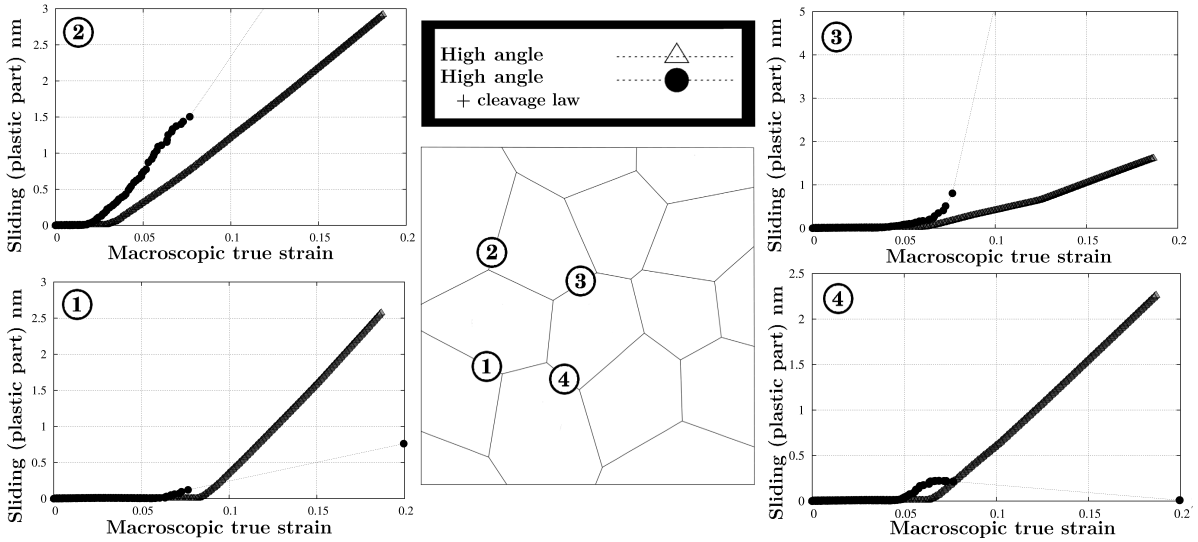

FIG. 7: Plastic part of sliding vs macroscopic true strain for four nodes numbered from 1 to 4 for HA texture under tension with and without cleavage law.

4 Conclusion

In this work, a two-scale method accounting for the specific GBCD of nc copper was developed. Such method does not suffer from the length scales limitations commonly encountered in atomistic simulations. Note that this methodology can also be used for other materials such as brittle ceramics, where GB deformation plays an important role on their mechanical responses.

GBs elasto-plastic laws of the misorientations of grains for two different textures LAB and HAB were extracted from QC calculations and used in a RVE. Both HAB and LAB samples were subjected to tensile tests and the comparison of their mechanical behaviors highlights their strong dependence on the texture. LAB texture presents a much higher yield stress than in the HAB texture. A unique decohesion law was incorporated in the HA texture tensile test to highlight the role played by GB opening on the microstructure. A loss of strain energy and a lower yield stress of the overall microstructure was found as expected.

It must finally be emphasized that the results remain overvalued compared to dynamic molecular simulations. The discrepancy can easily be rationalized by the fact that voids and surface defects and thermally activated processes are not accounted for in the simulations, and

that plasticity is restricted here to GBs. Future work includes misorientation GBCD dependent cleavage law, the incorporation of defects in the GB in the QC simulations and the consideration of anisotropic intragranular plasticity.

5 Bibliography

Références

[1] V. Péron-Lührs, A. Jérusalem, F. Sansoz, L. Stainier, and L. Noels. A two-scale model predicting the mechanical sliding behavior of grain boundaries in nanocrystalline solids. *Submitted to Journal of the Mechanics and Physics of Solids*, 0 :0, 2011.

[2] H. Gleiter. Nanostructured materials: basic concepts and microstructure. *Acta Materialia*, 48 :1–29, 1999.

[3] G. E. Fougere, J. R. Weertman, and R. W. Siegel. Processing and mechanical behavior of nanocrystalline fe. *Nanostructured Materials*, 5 :127–134, 1995.

[4] E. Bitzek, P. M. Derlet, P. M. Anderson, and H. Van Swygenhoven. The stress-strain response of nanocrystalline metals : A statistical analysis of atomistic simulations. *Acta Materialia*, 56 :4846–4857, 2008.

[5] V. B. Shenoy, R. Miller, E. B. Tadmor, D. Rodney, R. Phillips, and M. Ortiz. An adaptive finite element approach to atomic-scale mechanics: the quasicontinuum method. *Journal of the Mechanics and Physics of Solids*, 47 :611–642, 1999.

[6] A. Jérusalem, L. Stainier, and R. Radovitzky. A continuum model describing the reverse grain-size dependence of the strength of nanocrystalline metals. *Philosophical Magazine*, 87 :2541–2559, 2007.

[7] M. Ortiz and A. Pandolfi. Finite-deformation irreversible cohesive elements for three-dimensional crack-propagation analysis. *International Journal for Numerical Methods in Engineering*, 44 :1267, 1999.

[8] D.H Warner, F. Sansoz, and J.F. Molinari. Atomistic-based continuum modeling of deformation mechanisms in nanocrystalline copper. *International Journal of Plasticity*, 22 :754, 2006.

[9] F. Sansoz and J. F. Molinari. Mechanical behavior of σ tilt grain boundaries in nanoscale Cu and Al: A quasicontinuum study. *Acta Materialia*, 53 :1931–1944, 2005.

[10] F. Sansoz and J. F. Molinari. Incidence of atom shuffling on the shear and decohesion behavior of a symmetric tilt boundary in copper. *Scripta Materialia*, 50 :1283–1288, 2004.

[11] L. Li and N. M. Ghoniem. Twin-size effects on the deformation of nanotwinned copper. *Physical Review B*, 79 :075–444, 2008.

[12] A. J. Cao and Y. G. Wei. Formation of fivefold deformation twins in nanocrystalline face-centered-cubic copper based on molecular dynamics simulations. *Applied Physics Letters*, 89 :4, 2006.